Journal of ELECTRONIC MATERIALS
DOI: 10.1007/s11664-017-5811-3

Electronic and Magnetic Structures, Magnetic Hyperfine Fields and Electric Field Gradients in UX_3 (X = In, Tl, Pb) Intermetallic Compounds

SAJID KHAN,[1,2,3,7] MAJID YAZDANI-KACHOEI,[4,8] SAEID JALALI-ASADABADI,[4] MUHAMMAD BILAL FAROOQ,[1,5] and IFTIKHAR AHMAD[1,6]

1.—Center for Computational Materials Science, University of Malakand, Chakdara 18800, Pakistan. 2.—Department of Physics, University of Malakand, Chakdara 18800, Pakistan. 3.—Govt Post Graduate College, Charsadda 24420, Pakistan. 4.—Department of Physics, Faculty of Sciences, University of Isfahan, Hezar Gerib Avenue, Isfahan 81746-73441, Iran. 5.—Department of Physics, Abbottabad University of Science and Technology, Havelian, Abbottabad 22500, Pakistan. 6.—Abbottabad University of Science and Technology, Havelian, Abbottabad 22500, Pakistan. 7.—e-mail: skhan.ccms@gmail.com. 8.—e-mail: yk.majid@gmail.com

Cubic uranium compounds such as UX_3 (X is a non-transition element of groups IIIA or IVA) exhibit highly diverse magnetic properties, including Pauli paramagnetism, spin fluctuation and anti-ferromagnetism. In the present paper, we explore the structural, electronic and magnetic properties as well as the hyperfine fields (HFFs) and electric field gradients (EFGs) with quadrupole coupling constant of UX_3 (X = In, Tl, Pb) compounds using local density approximation, Perdew–Burke–Ernzerhof parametrization of generalized gradient approximation (PBE-GGA) including the Hubbard U parameter (GGA + U), a revised version of PBE-GGA that improves equilibrium properties of densely packed solids and their surfaces (PBEsol-GGA), and a hybrid functional (HF-PBEsol). The spin orbit-coupling calculations have been added to investigate the relativistic effect of electrons in these materials. The comparison between the experimental parameters and our calculated structural parameters we confirm the consistency and effectiveness of our theoretical tools. The computed magnetic moments show that magnetic moment increases from indium to lead in the UX_3 family, and all these compounds are antiferromagnetic in nature. The EFGs and HFFs, as well as the quadrupole coupling constant of UX_3 (X = In, Tl, Pb), are discussed in detail. These properties primarily originate from f and p states of uranium and post-transition sites.

Key words: Structural properties, state-of-the-art calculations, magnetic properties, hyperfine field (HFF), electric field gradient (EFG), quadrupole coupling constant

INTRODUCTION

The actinides and their compounds show dual magnetic properties and cover a wide range of magnetic states that vary from 4f localized behavior to 3d itinerant band-like character. This two-fold variety is due to the more extensive 5f electron wave function of uranium relative to the lanthanides. Cubic uranium compounds such as UX_3, where X is a non-transition element of groups IIIA or IVA, are interesting intermetallic compounds. These compounds exhibit great diversity in their magnetic properties, such as Pauli paramagnetism in USi_3 and UGe_3, spin fluctuations in UAl_3 and USn_3 and

(Received June 28, 2017; accepted September 13, 2017)

local moment antiferromagnetic ordering in UIn_3, UTl_3 and UPb_3.[1] These compounds show an $AuCu_3$ - type crystal structure, where the uranium atomic space d (U-U) is the same as the lattice constant of the unit cell. It has been noted that the d (U-U) of such compounds are remote from the Hill limit (3.25–3.5 Å); consequently, 5f ligand hybridization constitutes the primary mechanism for controlling the 5f electrons.[2,3] Hill et al. showed that the 5f electrons could behave similarly to band electrons and are not localized. The authors also concluded that protactinium was the primary element in the actinide series for which the 5f state is populated; hence, Pa metal should be the first proper 5f transition element. Kmetko et al. and Johansson et al. noted that the latter part of the series beginning with americium must be considered as localized systems. Therefore, they regarded Am as the leading member of the heavier actinide series which resembles the rare-earth metals.[4,5] The actinides and their compounds include superatomic clusters that exhibit a unique electronic structure as well as optical and magnetic properties due to their hyperactive 5f valence electrons.[6–8]

The electronic specific heat of actinide intermetallic compounds UX_3 varies as a result of the f–p hybridization interaction. The electronic specific heat coefficient γ of UIn_3 and UPb_3 are 40 mJ/K^2 mol, and 110 mJ/K^2 mol, respectively. Maaren et al. found the experimental electronic specific heat to be 50 mJ/K^2 mol for UIn_3.[9–12] Murasik et al. determined that UIn_3, UTl_3 and UPb_3 should be antiferromagnetic with magnetic moments of 1 μ_B, 1.6 μ_B, and 1.7 μ_B, respectively.[13,14] The Néel temperature determined by Tokiwa et al. for UIn_3, UTl_3 and UPb_3 is 88 K, 90 K, and 30 K, respectively.[11] The electric field gradient (EFG) is also an important parameter which links condensed matter physics to nuclear physics. The EFGs of 4f and 5f rare-earth and actinide dipnictides were computed by Jalali-Asadabadi et al.[8,15–17] and Yazdani-Kachoei et al.[18]

Before contemplating the origin of the observed trend and attempting to understand the physical properties of UX_3, a thorough knowledge of the 5f electrons is necessary. In this paper we present the basic hybridization processes which give rise to the narrow-band structure and the delocalization of f electrons at the Fermi level. Few studies have investigated the structure, electronic specific heat, magnetic moment, electric field gradient, quadrupole coupling constant and interaction energy resulting from the complex behavior of the uranium 5f states. Therefore, in this work we study these parameters using the full-potential augmented plane wave, including the local (FP-APW + lo) method, with the addition of spin–orbit coupling.

Special consideration has been given to the following questions (1) Which contributions of orbital, Fermi contact and spin-dipolar, dominates the magnetic hyperfine fields (HFFs) at uranium indium, thallium and lead sites? (2) Which orbitals take part in magnetism? (3) What is the origin of nonzero HFFs at U, In, Tl and Pb sites? (4) Which electron predominantly contributes to the EFG at U, In, Tl and Pb sites? (5) Which states play a central role in the hybridization processes that take place in UX_3 compounds? (6) What are the nuclear quadrupole coupling constants of In, Tl, and Pb sites?

COMPUTATIONAL DETAILS

The structural, electronic, and magnetic properties as well as the electric field gradient and hyperfine field of UX_3 (X = In, Tl, Pb) are investigated using the (FP-APW + lo) method as embodied in the WIEN2k package.[19] This is one of the most accurate schemes for the investigation of the different properties of solids. In this method, the crystal cell is separated into two regions, i.e., nonoverlapping atomic muffin-tin spheres with R_{MT} radii and interstitial region. The wave functions within muffin-tin spheres are expanded in spherical harmonics, while the interstitial region is expanded in terms of plane waves.[20,21] In this work, we deal with UX_3 (X = In, Tl, Pb) compounds that behave as strongly correlated systems. The structural properties are investigated under the (LDA) and GGA (PBEsol).[22,23] The magnetic properties of these heavy fermion materials have been investigated under the consideration of GGA + U in which an additional Hubbard-U term is added with a hybrid functional HF-PBEsol. We found in this study that the GGA + U (with $U \approx 7$ eV) approach provides an improved description of the magnetic properties of UX_3 compounds.[24–27] Our recent calculations of UX_3 (X = In, Tl, Pb) are also computed using exact exchange for correlated electrons. The EECE gives good results in the case of UX_3 with $\alpha = 0.01$. Moreira et al. suggested the hybrid functional with the following general form:

$$E_{xc}^{\text{onsite}-\text{HF}}[\rho] = E_{xc}^{SL}[\rho] + \alpha\left(E_x^{HF}[_{\text{core}}] - E_x^{SL}[\rho_{\text{core}}]\right), \quad (1)$$

where E_{xc}^{SL} is the semilocal (SL) functional, and α is the fraction of Hartree–Fock exchange (between 0 and 1).[28–30] Because uranium has a large number of fermions, spin orbit-coupling calculations are necessary to thoroughly define its properties.

The radii of the MT spheres were selected as 2.7 a.u. for U atom and 2.4 a.u for X = In, Tl, Pb atoms. These optimized values provide stability in the structural and magnetic calculations. To provide satisfactory results we selected 2000 k-pints for UX_3. In the MT spheres, expansion of the wave function was limited to a maximum angular momentum quantum number l_{max} = 10. The expansion of the interstitial region wave function was limited to a cutoff plane wave of $K_{max} = 9/R_{MT}$, where R_{MT} is the minimum muffin-tin radius in the crystal unit cell, while the selected Fourier expansion of the density is limited by the cutoff G_{max} = 12. The selected convergence criteria for energy and charge are 0.0001.

RESULT AND DISCUSSION

Structural Properties

UX_3 [*U* = In, Tl, Pb] compounds show $AuCu_3$ -type face-centered cubic structures with a space group of Pm-3 m (221) and atomic positions of *U* in 1 (a); [0, 0, 0] and X in 2 (d); [0.5, 0.5, 0.0]; [0.0, 0.5, 0.5] and [0.5, 0.0, 0.5]. The experimental lattice constants of UIn_3, UTl_3, and UPb_3 are 4.601 Å, 4.674 Å, and 4.792 Å, respectively.[2,3] We used experimental lattice constants and relaxed the crystal by minimizing the total energy versus unit cell volume and fitted the results with a Birch–Murnaghan equation of states.[31] To obtain the optimized structural parameters of UX_3 compounds we used the local density approximation as well as a generalized gradient potential that were implemented in WIEN2k package. We first optimized the unit cell UX_3 using LDA and GGA (PBEsol) and obtained the structural parameters including lattice constants, bulk moduli, pressure derivatives and interatomic distance between U-U and U-X. The computed information is tabulated in Table I, while plots of the energies versus the volume of UX_3 are shown in Fig. 1a, b, and c.

Our results show that lattice parameters calculated by GGA are more consistent with experimental results compared to LDA as shown in Fig. 2a, which displays the effectiveness of GGA for the structural properties of the UX_3 family. The results of LDA are underestimated due to the absence of correlation effects, which gives rise to a tendency toward over-binding and smaller lattice constants.[32,33] The bulk modulus, which defines the strength of a material, has been investigated using different functionals. Figure 2b shows the bulk modulus of these materials. The lattice constants of these compounds increases upon moving from In to Pb, while the bulk moduli decrease in the UX_3 series, which satisfies the inverse relation between bulk modulus and lattice constant. In other words, the softness of the materials increases from In to Pb, and UIn_3 is the hardest material in this family.

Thus we have concluded that UIn_3 is the hardest and least compressible of the UX_3 series. We also calculate the pressure derivatives B' of the bulk modulus, which is an important parameter of great physical significance in the study of high-pressure physics.[34] The magnetic behavior of UX_3 has been verified by minimizing the unit cell volume versus energy. We conclude that UX_3 materials contain less energy in their antiferromagnetic structure, specifically, − 182871.984323 Ry for UIn_3, − 355705.196109 Ry for (UTl_3) and − 363380.838078 Ry for (UPb_3). Knowledge of the interionic spacing between U-U and U-X is important when seeking to understand the structure and delocalization of electrons in actinide $AuCu_3$ compounds. As the U-U spacing exceeds the Hill limit, the delocalizing effect of f–f overlap diminishes, but f-spd hybridization may still prevent the formation of stable local moments in UX_3 compounds.[35] The calculated bond lengths of U-U and U-X coincide with experimental results. The U-In bond length is smaller than the other bond lengths in the series, and this leads to greater hardness and a larger bulk modulus. Computations show that smaller bond lengths between

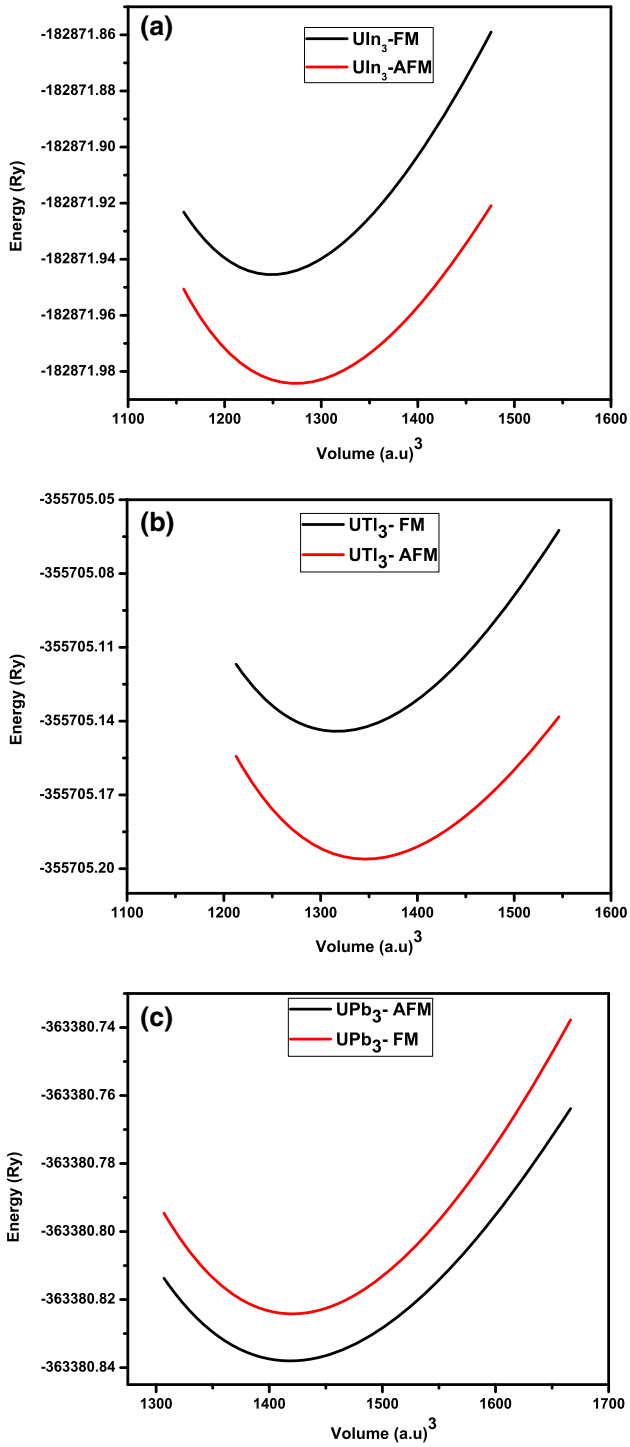

Fig. 1. (a) Variation of energy versus volume for the cubic unit cell of UIn_3, (b) UTl_3, and (c) UPb_3 in both the FM and AFM phases.

Table I. Comparison of calculated lattice constants (Å), bulk moduli (GPa), derivatives of bulk moduli, double cell ground state energy as well as the interatomic space between U-U and U-X by different potentials and comparison with the experimental results

	LDA	GGA (PBsol)	Exp	% Err GGA
UIn_3				
Lattice	4.4994	4.5475	4.601[a,b]	1%
Pressure	89.1131	79.9534		
Volume	91.088554859784	94.041191546875	97.399493801	3.4%
P derivative	5.0000	5.0000		
Ferro		− 182871.945462		
Anti-Ferro		− 182871.984323		
U-U			4.601[a,b]	
Exp U-In			3.253[a,b]	
GGA U-U		4.6020		
GGA U-In		3.25411		3.253
UTl_3				
Lattice	4.5945	4.6421	4.674[a,b]	0.6%
Pressure	84.1395	76.355		
Volume	96.987277283625	100.033041876461	102.10949402	2.0%
P derivative	5.000	5.000		
Ferro		− 355705.144265		
Anti-Ferro		− 355705.196109		
U-U			4.674[a,b]	
Exp U-In			3.306[a,b]	
GGA U-U		4.6740		
GGA U-Tl		3.30502		
UPb_3				
Lattice	4.6688	4.7158	4.792[a,b]	1.5%
Pressure	77.2868	69.4912		
Volume	101.769071132672	104.873589868312	110.039961088	4.6%
P derivative	5.00	5.00		
Ferro		− 363380.824292		
Anti-Ferro		− 363380.838078		
U-U			4.792[a,b]	
Exp U-In			3.388[a,b]	
GGA U-U		4.79200		
GGA U-Pb		3.38846		

[a]Reference 2.[b]Reference 3.

U-X lead to greater bulk moduli for the UX_3 family, as shown in Table I.

Electronic Band Structure and Electronic Specific Heat of UX_3 (X = In, Tl, Pb)

Both the electronic band structure and density of states calculations are important when investigating the metallic nature of UX_3 (X = In, Tl, Pb) compounds. The electronic band structure has been calculated by GGA + U including spin–orbit coupling. As shown in Fig. 3a, b, and c, the valence and conduction band cross each other around the Fermi level, which clearly indicates the intermetallic nature of uranium binary compounds. The knowledge derived from DOS is very important when computing the electronic specific heat at low temperatures. In a conventional metal, the electronic specific heat can be related to the density of states at the Fermi level by the following equation:

$$\gamma = \frac{\pi^2}{3} k_B^2 \mathrm{DOS}(E_F), \tag{2}$$

where k_B is the Boltzmann constant and DOS (E_F) is the density of states at the Fermi energy in states/eV.[36] In order to investigate the Sommerfeld coefficient or the electronic specific heat in UX_3 compounds, we calculated the densities of states (DOS) of the compounds under study using the different exchange–correlation approaches GGA + U and HF-PBEsol in the absence and presence of spin orbit coupling calculations as shown in Fig. 4.

It is clear from Fig. 4 that electrons belonging to the outermost 5*f* orbital of uranium as well as the 5*p* and 6*p* orbitals of indium, thallium and lead primarily contribute to bond formation, and there exists *f*–*p* hybridization with uranium states which leads to overlap of the valence and conduction band at the Fermi level. The overlap of the valence and

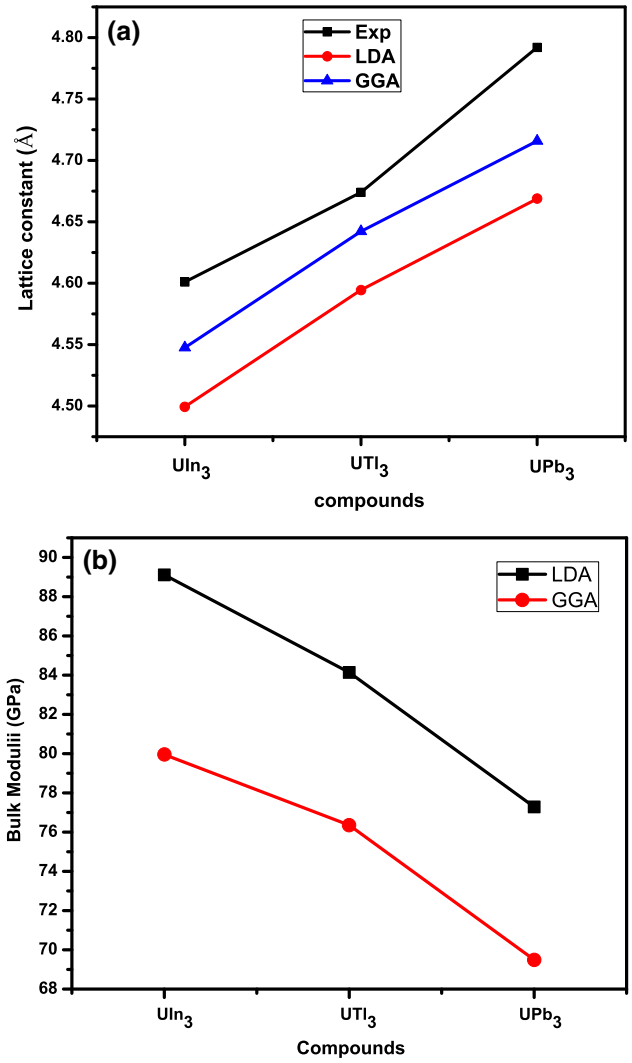

Fig. 2. (a) Calculated and experimental lattice constants, and (b) calculated bulk moduli of the UX_3 compounds (X = In, Tl, Pb).

conduction band with the addition of 5f electrons across the Fermi level confirms the metallic nature of these compounds. As shown in the Fig. 4, the SOC increased the number of density of states at the Fermi level, which is in consistence with the experimental value. This means that the SOC improves the specific heat for the actinide family. The results of the electron specific heat calculations are given in Table II. The electronic specific heat coefficient calculated with HF-PBEsol + SOC is close to experimental value.[12,37] The total DOS has a large limited value at the Fermi level (E_F), which is equal to 24.2 states/eV, 53 states/eV, and 49.7 states/eV per unit cell in UX_3 (X = In, Tl, Pb). As shown in Fig. 4, the 5f state crosses the Fermi level, and this confirms the intermetallic nature of UX_3. The 5f state electrons of uranium primarily contribute to the specific heat. The γ values derived from HF-PBEsol with SOC calculations are 55 mJ/mol K^2, 122 mJ/mol K^2, and 112 mJ/mol K^2 for UX_3 (X = In, Tl, Pb). It is clear from Fig. 4 that core electrons contribute to the valence band, while conduction is due to unfilled *f*- and *p*-state electrons, as well as slight f-spd hybridization. The overlap of valence and conduction bands once again confirms the metallic nature of UX_3 compounds.

Magnetic Nature of UX_3 [X = In, Tl, Pb]

It is necessary to study the magnetic properties of UX_3 (X = In, Tl, Pb)because of the 5f electrons, which not only contribute to the metallic nature but also exhibit the magnetic moments. The electronic configuration of uranium is $6p^6\ 5f^3\ 6d^1\ 7s^2$ while the electronic configurations of In, Tl and Pb are $4p^6\ 4d^{10}\ 5s^2\ 5p^1$, $5p^6\ 5d^{10}\ 6s^2\ 6p^1$, and $5p^6\ 5d^{10}\ 6s^2\ 6p^2$, respectively. It is generally accepted that the direct 5f-wave function overlap and hybridization with the ligand states constitute the two predominant contributions to the formation of the 5f-band of actinide systems. To examine the interstitial and individual atomic spin magnetic moments per unit cell of UX_3 (X = In, Tl, Pb) different functionals, such as GGA + U and HF-PBEsol, were utilized. For actinide systems, spin–orbit coupling is not negligible, and the orbital magnetic moments have large magnitudes. Therefore, we also performed a calculation under the consideration of GGA + U+SOC as well as HF-SOC flavors.[38,39] The calculated values of spin, orbital and total magnetic moments for UX_3 by GGA + U and HF-PBEsol in the absence and presence of SOC are shown in Table III, along with the experimental results. The calculated spin and orbital magnetic moments for the actinides have opposite signs, which indicates that both are antiparallel, and the resultant magnetic moment is minute. In this study, spin and orbital moments are anti-parallel to each other in UX_3, hence such systems fulfill Hund's third rule $J = |L - S|$. The GGA + U with SOC gives the total magnetic moments at the uranium site as 1 μ_B/U (UIn_3), 1.4 μ_B/U (UTl_3) and 1.6 μ_B/U (UPb_3), respectively, which is consistent with the experimental results.[13,14]

The calculated magnetic moments are arranged as follows. The orbital and spin moment on the uranium, indium, thallium and lead site are opposite in direction. As shown in Table III, the spin magnetic moment is smaller than the orbital magnetic momentat uranium site, and the total magnetic moment per unit cell is reduced as a result. The calculated partial DOS around the Fermi energy, as presented in Fig. 4, shows that the moment of uranium is almost exclusively of 5f character, and the moment of indium, thallium and lead is primarily 5*p* and 6*p* in character.

As shown in Fig. 5a, the calculated magnetic moments at the uranium site differ from experimental data for all potentials with the exception of the results derived from GGA + U including spin orbit coupling. The total magnetic moment per unit cell has been calculated as shown in the Table III,

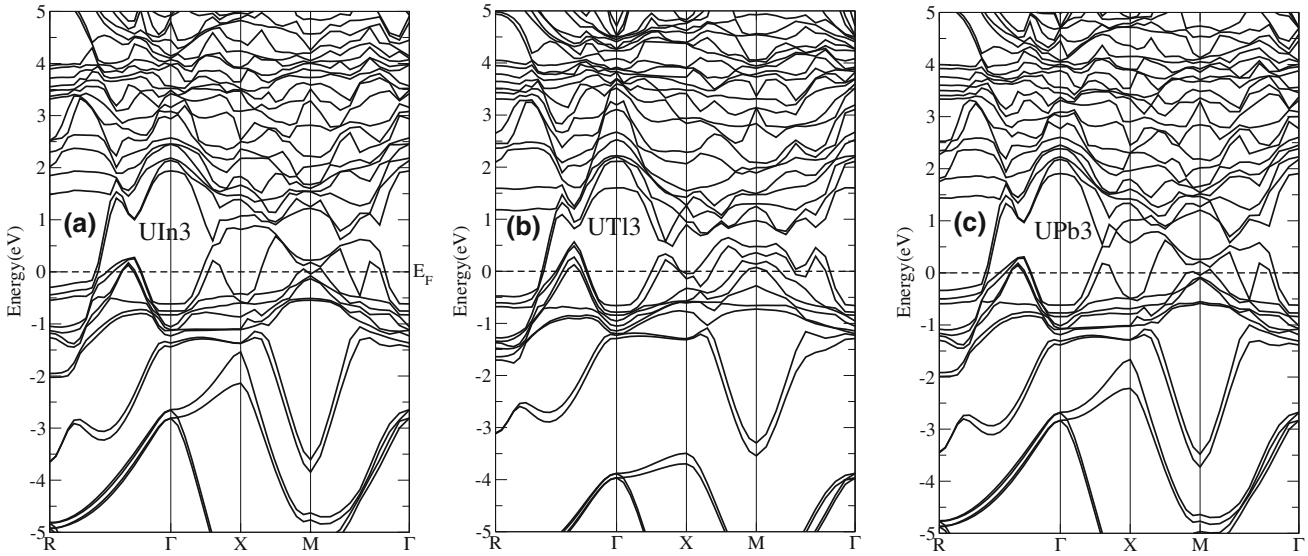

Fig. 3. (a, b, c) Electronic band structure for $AuCu_3$ -type cubic UX_3 (X = In, Tl, Pb) compounds by GGA + U + SOC.

Table II. The electronic specific heat of UX_3 (X = In, Tl, Pb)

	UIn_3	UTl_3	UPb_3
GGA + U	32.2	55.2	7.0
HF-PBEsol	33.12	108	57.5
GGA + U+SOC	46	73.6	55.2
HF-PBEsol + SOC	55.5	122	114
Exp. γ	50[a,b]		110[a,b]

[a]Reference 11.[b]Reference 12.

and the corresponding figure, Fig. 5b. The total magnetic moment at the actinide site calculated using GGA + U + SOC increases from 1 μ_B to 1.7 μ_B with increasing atomic number and lattice constant, which is in agreement with the experimental results. Experimental data regarding the individual orbital and spin contributions as well as total magnetic moment per unit cell does not exist. Thus, our results serve as a prediction for UX_3. The UX_3 compounds categorized in cubic $AuCu_3$ form exhibit inter-atomic distances d_{Ac-Ac} by GGA of 4.601 Å, 4.674 Å, and 4.792 Å, which are far away from critical Hill limit of 3.4 Å. Thus 5*f* electrons are strongly delocalized by direct overlap that magnetic order can no longer be supported and materials exhibit antiferromagnetic intermetallic nature. The inter-atomic separation of uranium atom is larger than Hill limit so this material has intermetallic magnetic nature. The Hill limit leads to direct 5*f* electron overlap between neighboring uranium atoms as well as strong hybridization with electrons of the alloying partner. However, at large Ac–Ac separations, 5*f* delocalization is only possible by hybridization with ligand orbitals as the separation is more than the Hill limit. Therefore, the antiferromagnetic nature of this family is due to the hybridization of f and ligand orbitals (*s–p–d*).[40,41]

Hyperfine Field (HFF) and Electric Field Gradient (EFG)

The hyperfine field (HFF), electric field gradient (EFG), nuclear quadrupole coupling constant (NQCC) and asymmetry parameter (η) of the atomic nuclei are very important in various research fields. These parameters measure the electric quadrupole interaction, which is a central investigatory tool in many areas of condensed matter physics as well as in biological materials. These parameter measure the deviation of nuclear charge distribution from spherical symmetry.[42]

Magnetic hyperfine as well as electric quadrupole interactions are important when seeking to understand the nature of the electron cloud and nucleus. The nuclear magnetic dipole moment μ_N and the extra magnetic field generated by the electron cloud gives rise to the magnetic hyperfine fields. The interaction of nuclear spin $\vec{I}$ located at $r = 0$ with orbital $\vec{l}$ and electron spin $\vec{s}$ is

Table III. Calculated spin (μ_{spin}), orbital (μ_{orb}) and Ñ ($\mu_{tot} = \mu_{orb} + \mu_{spin}$) in terms of the Bohr magneton (μ_B) of UX_3 (X = In, Tl, Pb) using GGA + U and HF-PBEsol in the absence and presence of spin orbit-coupling

		Magnetic moment							
		GGA + U	HF-PBEsol	GGA + U + SOC			HF-PBEsol + SOC		
Compounds	Sites	μ_{spin}	μ_{spin}	μ_{spin}	μ_{orb}	$\lvert\mu_{tot}\rvert$	μ_{spin}	μ_{orb}	$\lvert\mu_{tot}\rvert$
UIn_3	M^{int}	0.253	0.315	0.237	0.000	0.000	0.034		
	M^{U}	2.821	2.258	2.775	− 3.865	1.090	1.954	− 2.642	0.680
	M^{In}	− 0.007	− 0.012	− 0.013	− 0.001	0.013	− 0.012	− 0.003	0.015
	M^{In}	− 0.008	− 0.013	− 0.021	− 0.001	0.021	− 0.017	− 0.003	0.020
	M^{tot}	3.059	2.609	2.966	− 3.866	0.898	2.333	− 2.65	0.320
	U-U	4.601							
Exp: $_B$/U	1.0[a,b]								
UTl_3	M^{int}	0.249	0.278	0.188	0.000	0.000	0.323		
	M^{U}	2.828	2.338	2.048	− 3.314	1.300	2.069	− 2.919	− 0.85
	M^{Tl}	− 0.003	0.004	− 0.003	− 0.001	0.003	− 0.007	− 0.002	0.009
	M^{Tl}	− 0.003	− 0.003	− 0.001	− 0.001	0.001	− 0.007	− 0.002	0.009
	M^{tot}	3.070	2.627	2.242	− 3.315	1.074	2.410	− 2.923	0.505
	U-U	4.674							
Exp: $_B$/U	1.6[a,b]								
UPb_3	M^{int}	0.218		0.235			0.206		
	M^{U}	2.939	2.709	2.700	− 4.259	1.558	1.771	− 2.735	1.00
	M^{Pb}	− 0.002	− 0.006	− 0.002	− 0.003	0.005	− 0.005	− 0.001	0.005
	M^{Pb}	− 0.002	− 0.007	− 0.002	− 0.003	0.005	− 0.004	− 0.001	0.005
	M^{tot}	3.154	2.862	2.932	− 4.264	1.334	1.963	− 2.737	
	U-U	4.792							
Exp: $_B$/U	1.7[a,b]								

[a]Reference 13.[b]Reference 14.

$$H_{FF}^{tot} = 2\mu_B\gamma_\rho\hbar\vec{I}\left[\frac{\vec{l}}{r^3} - \frac{\vec{s}}{r^3} + 3\frac{(\vec{r}\vec{s})\vec{r}}{r^5} + \frac{8}{3}\pi\vec{s}\delta(\vec{r})\right] \quad (3)$$

The first term in the above equation corresponds to interaction with the orbital moment, while the second and third terms describe the interaction with the electron spin. The final term is the Fermi contact hyperfine interaction.[41] In addition to the hyperfine field, the second rank tensor electric field gradient is also an instructive parameter which clearly explains the distribution of electrons around the nucleus and the electric quadrupole interaction energy. The major component of EFG is V_{zz}, where

$$V_{zz} = \lim_{r\to 0}\left[\frac{5}{4\pi}\right]^{1/2}\left[\frac{V_{20}(r)}{r^2}\right] \quad (4)$$

Equation 4 shows that the major axis of the EFG tensor points in the z-direction, where V_{20} is the radial potential and can be calculated as

$$V_{20}(r=0) = \frac{4\pi}{5}\int_0^{R_{MT}}\frac{\rho_{20}}{r}dr - \frac{4\pi}{5}\int_0^{R_{MT}}\frac{\rho_{20}}{r}\left(\frac{r}{R_{MT}}\right)^5 dr + 4\pi\sum_k V(k)J_2(kR_{MT})Y_{20}\left(\hat{k}\right) \quad (5),$$

where the first (second and third) term in Eq. 5 correspond to the valence (lattice) contribution toward EFG, while $J_2(kR_{MT})$ is the spherical Bessel function, and R_{MT} is the Muffin-tin (MT) sphere radius. The EFG at a given site can be different for different materials. Therefore, many researchers consider the EFG to be a fingerprint for each compound.[17,42–45] Theoretically, knowledge of the EFGs at the atomic sites predicts the U, In, Tl, and Pb nuclear quadrupole coupling constant (NQCC), which enables calculation of the electric quadrupole interaction energy. The HFF and EFG can be measured directly or indirectly by a number of experimental methods, such as the perturbed angular correlation, nuclear magnetic resonance or Mössbauer spectroscopy.[16] In this work, special consideration has been devoted to the questions that could not be answered by the experimentalist, including (1) Which orbital is the major contributor to HFF? (2) Which contribution of core, valence, orbital and dipole dominates in the magnetic HFF? (3) What is the origin of a nonzero HFF at uranium, indium, thallium and lead sites? (4) Which atom dominates EFG in the UX_3 family? To calculate HFF as well EFG, we used the FP-LAPW method as implemented in WIEN2k scheme. The calculated total HFF and its partial components, along with EFG, are presented in Tables IV and V for individual atoms of UX_3 (X = In, Tl, Pb) using GGA

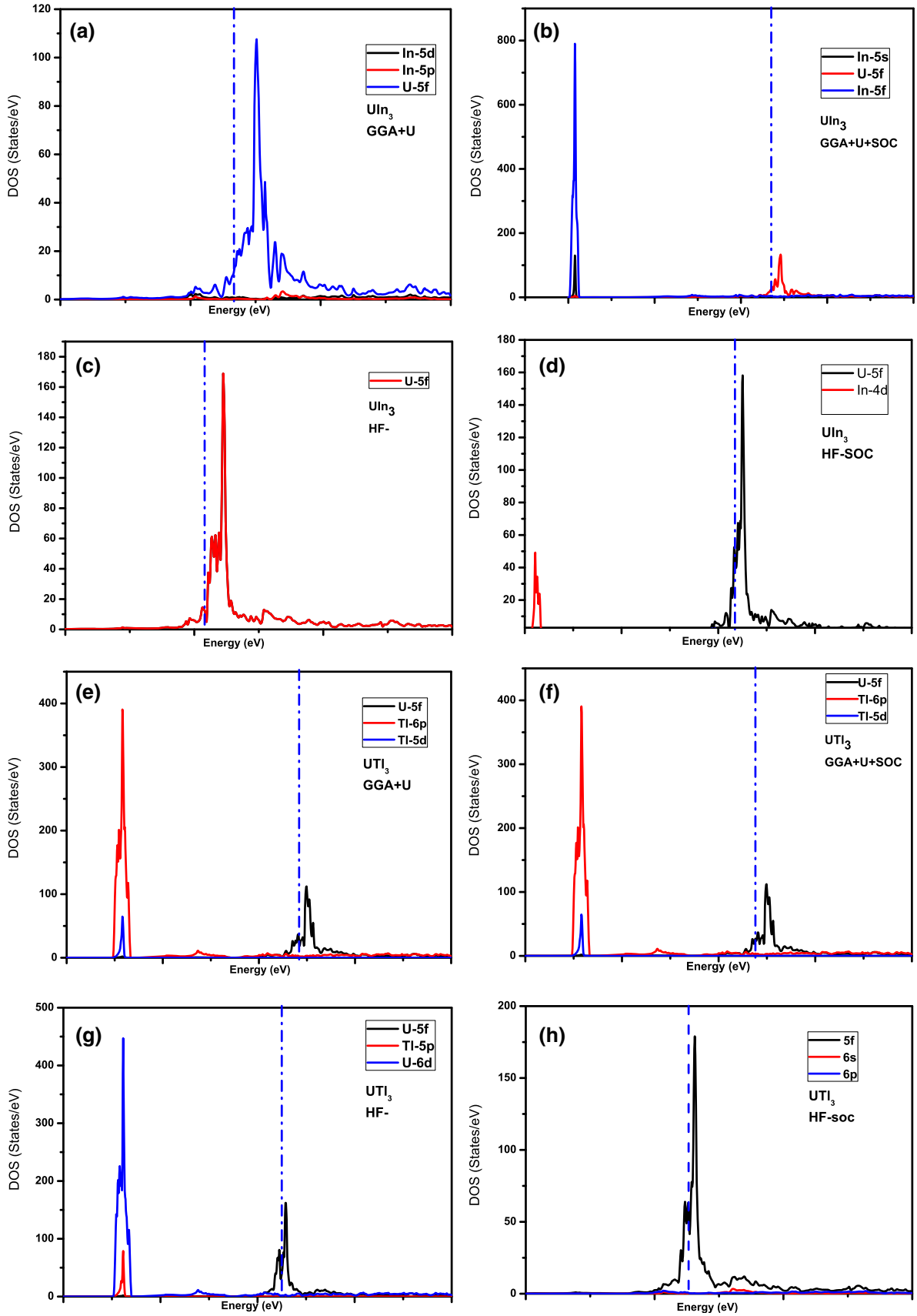

Fig. 4. (a, b, c, d, e, f, g, h, I, j, k, l) DOS of UX_3 (X = In, Tl, Pb) using different functionals with and without SOC calculations. The vertical dashed lines indicate the Fermi level.

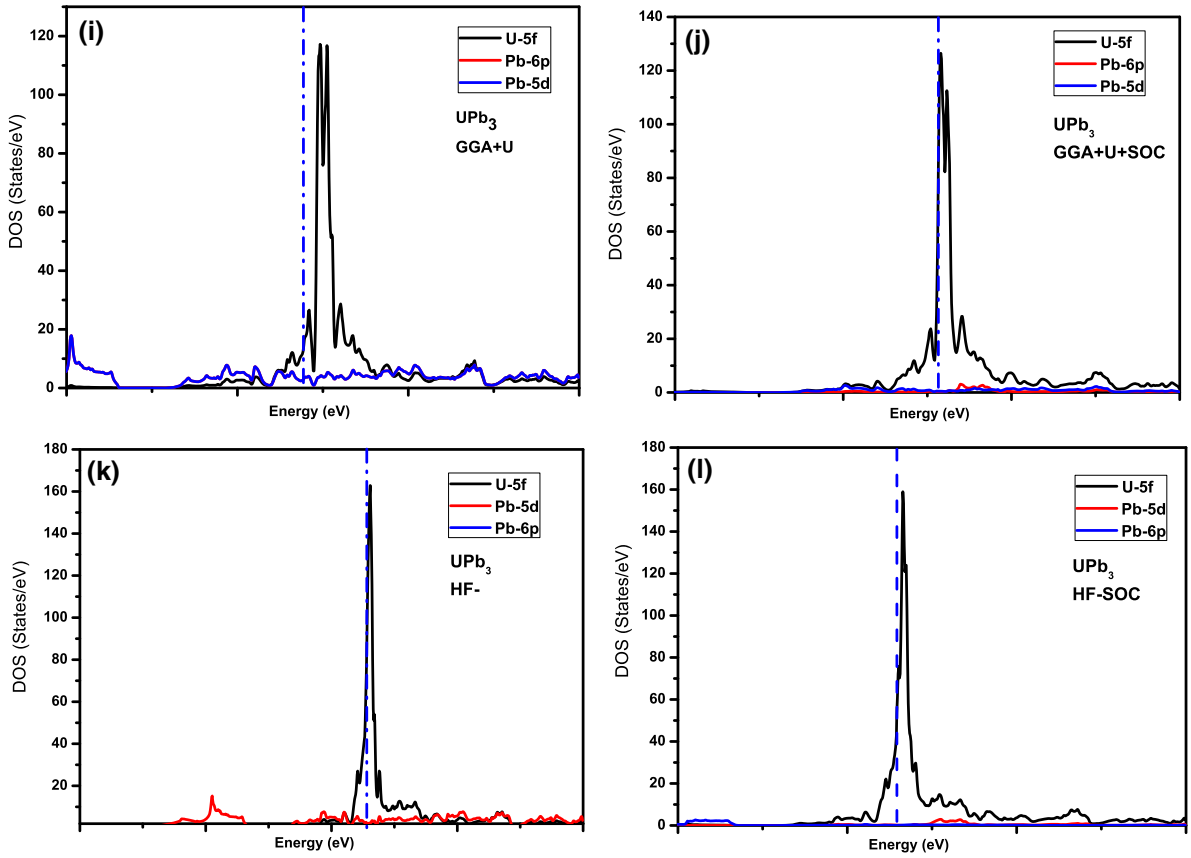

Fig. 4. continued.

and GGA + U in the presence of spin orbit coupling. The electron cloud around the nucleus generates a magnetic field which affect the nucleus site in the following manner. The electron has the property of spin, and its corresponding magnetic field reaches the nucleus in the form of a dipolar hyperfine field HFF^{dip}. The major contribution by this factor arises from the spin of *p* and *f* electrons at the uranium site, while *p* and *d* take dominancy in post-transition metals as shown in Fig. 6a and b. The dominant contributions to the total HFF derive from the orbital constituent. The electrons move in different orbitals which produces a magnetic moment like a current loop; the nucleus is subject to the effect of this magnetic field. The major rule contributed by the *p* orbital for both uranium and post-transition metals render its magnetic effect diffuse, allowing it to reach the atomic site as shown in Fig. 6a and b under different potentials. The addition of GGA + U slightly improves the hyperfine field, which is in accord with other studies.[46] The valence, core, dipolar as well as total HFFs of the UX_3 series has been calculated as shown in Fig. 7a and b. The calculated large orbital hyperfine field of the f states is in accord with the results of Mohanta et al.[45] The *d*-orbital electrons are oriented in such a way that the net effect is minute. The computed zal as well as the dipolar hyperfine fields of *s* electrons is zero, which agrees with Eq. 4. The orbital and dipolar hyperfine field are parallel to each other at the uranium site, which enhances the total HFF. The Fermi contact hyperfine field in the absence of the magnetic field has been calculated as shown in Table V. In order to understand the origin of the Fermi contact, the valence as well as the core hyperfine field has been calculated. The valence and core hyperfine fields orient opposite one another at the uranium site due to the difference between the magnetic dipole moment of the electrons of the core and valence shells which minimizes the total interaction. The Fermi contact field gradually increases from UIn_3 to UTl_3 upon descending the group and decreases from UTl_3 to UPb_3 along the period. The Fermi contact field rises with increasing EFG from UIn_3 to UTl_3. The large contact and the total HFF both exhibit large a delocalization of electron density around the thallium site where such a trend is also observed for other elements.[47] Because the spin, orbital and magnetic moments of post-transition metals are minute, the HFF will be negligible in comparison with uranium. The systematic increase of uranium HFF is due to the increase of magnetic moment from UIn_3 to UTl_3 at the uranium site.

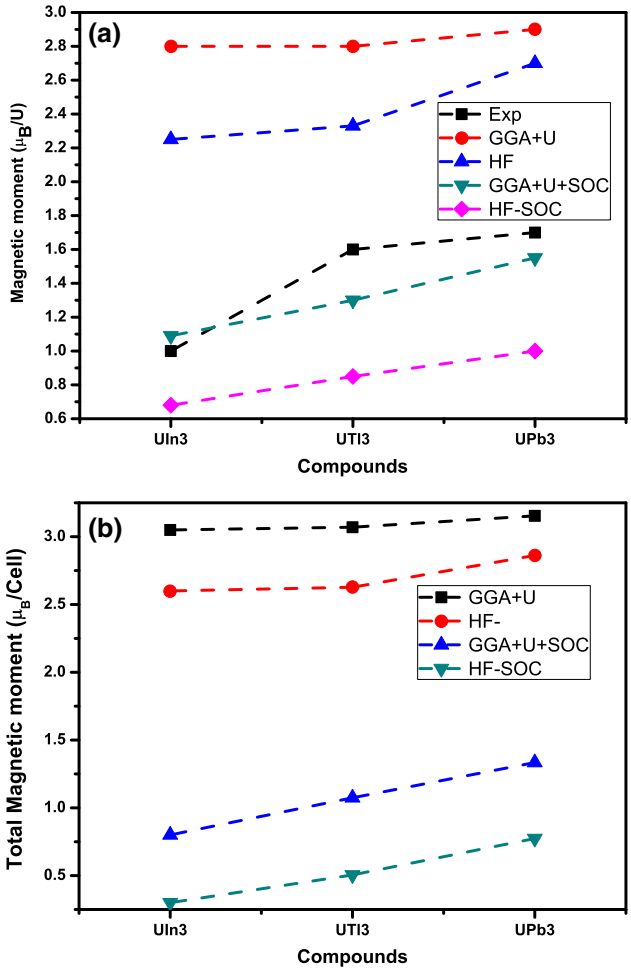

Fig. 5. (a) Variation of magnetic moment in Bohr magneton per uranium site in UX_3 family. (b) Calculated total magnetic moment per unit cell in UX_3.

The inner *s*- and polarized *f*-state electrons interact with each other and donate to the core hyperfine field, while the valence hyperfine field originates from the hybridization of local polarized f valence shell electrons with neighboring atoms. Hence, the Fermi contact HFF is determined from the contribution of local and neighboring atomic magnetic moments. It is suggested that the origin of the orbital and dipolar contributions of the HFF are exchange interaction between the p and f shells in uranium, while *p* and *d* orbitals contribute in indium, thallium and lead. Uranium, indium, thallium and lead have negative magnetic moments, which correspond to negative hyperfine fields. Experimental methods such as TDPAC, NMR and Mössbauer spectroscopy can measure the interaction energy between the quadrupole moment eQ of a nucleus and EFG at a particular site.

The interaction energy can be measured from the quadrupole coupling constant $C_Q = \frac{eQV_{zz}}{h}$, where eQ is the spectroscopic quadrupole moment (barn) of nuclei V_{ZZ} is the central component of the EFG tensor expressed in V/m^2.

The major component of EFG cannot be measured by direct experiment; however, if the nuclear electric quadrupole moment is known, V_{ZZ} can be obtained from C_Q. Otherwise, if V_{ZZ} is computed from first principles, a plot of the experimental C_Q versus the calculated V_{ZZ} should be a straight line with a slope determined by eQ. This is a way to measure a nuclear quadrupole moment using a combination of experimental and computational tools. The EFG at uranium and post-transition metals have been calculated using GGA + U in the absence and presence of spin–orbit coupling as shown in Table V. The total EFG (V_{zz}^{tot}) at the uranium site in UX_3 (X = In, Tl, Pb) calculated by GGA + U including spin orbit coupling are − 2.548 V/m^2, 1.95 V/m^2, and 0.6920 V/m^2. The total EFG at indium, thallium and lead sites are 15.95 V/m^2, 36.5260 V/m^2, and 34.94 V/m^2. According to our computed data the (V_{zz}^{tot}) at the uranium site increases from UIn_3 to UTl_3 and then decreases to UPb_3 for all the considered approaches. Similarly, the EFG gradually increases at the X site from the top to the bottom of the column and decreases from right to left in period. The large value of EFG at the thallium site is comparable to that of indium and lead because of the more extensive delocalization of 6p states, giving rise to a large aspherical charge distribution around the thallium site. The systematic change in the total EFG at the uranium site upon moving from UIn_3 to UTl_3 is mostly a volumetric effect. Since the interatomic distance of U-Tl is calculated to be more than that of U-In, the U 6d and 5f states are more itinerant in UTl_3 than UIn_3. As a result, the hybridization between U-(6d, 5f) and Tl-6p states is much smaller than the corresponding hybridization in UIn_3. The small EFG at the U site in UPb_3 provides a clear picture of the weak covalent interaction and the more spherical distribution of charge at the U site in UPb_3.

The EFG can be further grouped according to the different combinations of wave functions, namely *s*–*d*, *p*–*p*, *d*–*d* and *f*–*f* terms. It is proposed that the partial EFG *p*–*f* and s–*d* contributions of uranium in UX_3 (X = In, Tl, Pb) are minute compared to the *p*–*p*, *d*–*d* and *f*–*f* contributions. This illustrates that the most important contribution to EFG arises from electron wave functions with strong *p*–*p*, *d*–*d* and *f*–*f* character. The EFG at the In, Tl and Pb site are also shown in Table V, where the dominant contribution to the electric field gradient is due to *p*–*p* (5*p*–6*p*) and *d*–*d* (4*d*–5*d*) character, which verifies the aspherical electronic distribution and orbitals. In UX_3 (X = In, Tl, Pb) the post-transition metals showed complete 4*d* and 5*d* shells, and thus the *d* orbital is nearly spherically symmetric, while the *p* state exhibits more deviation from spherical symmetry.

The nuclear quadruple coupling constant C_Q is an important parameter used to calculate Mössbauer quadrupole splitting in atoms or molecules. The nuclear electric quadrupole moments eQ of quadrupole nuclei ^{115}In, ^{204}Tl and ^{207}Pb are 0.73, 0.74 and 0.34 barn, respectively.[42,48] To the best of our

Table IV. Dipolar and orbital hyperfine fields of UX_3 by GGA and GGA + U functionals with spin–orbit coupling

		Uranium site				X site (X = In, Tl, Pb)		
Site		***s***	***p***	***d***	***f***	***s***	***p***	***d***
Dipolar GGA								
UIn_3	up	0.0000	− 34.2570	− 0.96100	− 48.3710	0.0000	27.8132	1.01130
	dn	0.0000	− 174.720	− 01.1080	− 11.8320	0.0000	− 20.9587	1.11920
	net	0.0000	− 208.980	− 2.07000	− 60.2030	0.0000	6.85450	0.10800
UTl_3	up	0.0000	− 24.9658	− 0.81230	− 42.7720	0.0000	68.1753	− 3.08340
	dn	0.0000	− 182.455	− 1.18950	− 14.0360	0.0000	− 49.0433	3.3860 0
	net	0.0000	− 207.421	− 2.00170	− 56.8080	0.0000	19.1320	0.30260
UPb_3	up	0.0000	− 32.1124	0.02910	− 35.8686	0.0000	65.9215	− 1.42310
	dn	0.0000	− 111.291	− 1.11300	− 20.9694	0.0000	− 73.8809	1.76400
	net	0.0000	− 143.404	− 1.08380	− 56.8380	0.0000	− 7.95940	0.34090
Orbital GGA								
UIn_3	up	0.0000	− 210581	− 69.8671	− 1867.18	0.0000	− 34.5717	− 19.9380
	dn	0.0000	208,298	42.1045	44.6863	0.0000	32.1182	21.6961
	net	0.0000	− 2253.03	− 27.7626	− 1822.49	0.0000	− 2.45350	1.75770
UTl_3	up	0.0000	− 209234	− 76.7110	− 2023.17	0.0000	− 231.420	− 124.444
	dn	0.0000	206,883	44.5180	9.69310	0.0000	250.865	127.334
	net	0.0000	− 2350.91	− 32.1930	− 2013.48	0.0000	19.4457	2.88980
UPb_3	up	0.0000	− 207,804	− 92.3229	− 2033.14	0.0000	− 491.978	− 10.9893
	dn	0.0000	205,467	70.2845	101.630	0.0000	491.764	11.3993
	net	0.0000	− 2337.00	− 22.0384	− 1931.51	0.0000	− 0.21380	0.41001
Dipolar GGA + U								
UIn_3	up	0.0000	− 3.16140	− 0.08062	− 3.96636	0.0000	2.86712	− 0.09950
	dn	0.0000	− 18.2900	− 0.12728	− 1.25388	0.0000	− 2.11425	0.11120
	net	0.0000	− 21.4520	− 0.20790	− 5.22024	0.0000	0.75287	0.01170
UTl_3	up	0.0000	− 2.49490	− 0.08122	− 4.27700	0.0000	6.81768	− 0.30833
	dn	0.0000	− 18.2450	− 0.11896	− 1.40370	0.0000	− 4.90432	0.33860
	net	0.0000	− 20.7430	− 0.20018	− 5.68079	0.0000	1.91336	0.03027
UPb_3	up	0.0000	− 3.24298	0.00487	− 3.56418	0.0000	6.60863	− 0.14226
	dn	0.0000	− 11.3120	− 0.11331	− 2.09268	0.0000	− 7.40092	0.17677
	net	0.0000	− 14.5540	− 0.10843	− 5.65686	0.0000	− 0.79230	0.03450
Orbital GGA + U								
UIn_3	up	0.0000	− 21056.8	− 6.94567	− 185.140	0.0000	− 3.28170	− 2.01363
	dn	0.0000	20828.7	4.20255	4.57570	0.0000	3.22065	2.17055
	net	0.0000	− 228.080	− 2.74313	−180.560	0.0000	− 0.06100	0.15692
UTl_3	up	0.0000	− 209234	− 76.7110	− 2023.17	0.0000	− 232.230	− 126.761
	dn	0.0000	206,883	44.5180	9.69310	0.0000	254.654	130.234
	net	0.0000	− 2350.91	− 32.1930	− 2013.48	0.0000	22.4240	3.47300
UPb_3	up	0.0000	− 207850	− 9.32620	− 212.590	0.0000	− 49.7269	− 11.0110
	dn	0.0000	20546.1	6.85019	5.30177	0.0000	49.7088	11.3478
	net	0.0000	− 238.800	− 2.47610	− 207.280	0.0000	− 0.01204	0.33038

knowledge, there are no experimental EFG or C_Q values available for UIn_3, UTl_3 and UPb_3. There is little difference between the results of GGA + U with or without the addition of SOC calculation. The non-significant effect of the spin–orbit interaction on the EFG has also been observed by Divis et al. and Nourbakhsh et al.[49–51]

The quadrupole interaction energy at the atomic site is derived from aspherical 5f and 6p shells of electrons distributed around the nuclei of uranium in UX_3. The NQCCs of In, Tl and Pb are 288 MHz, 651 MHz, and 287 MHz, respectively. The major contribution to C_Q arises from the valence non-spherical $V_{zz}^{p\text{-}p}$ and $V_{zz}^{d\text{-}d}$ EFG. The quadrupole interaction energies at In, Tl and Pb are due to the eQ of nuclei and the corresponding valence EFG of 4p and 5p. The eQ and EFG interact with each other, and quadrupole interaction energy arises as a result. The quadrupole interaction energies at indium, thallium and lead sites are $\approx 1.19 \times 10^{-8}$ eV, $\approx 2.7 \times 10^{-8}$ eV, and $\approx 1.19 \times 10^{-8}$ eV, respectively. It has been suggested that the quadrupole interaction energy increases upon descending a column and decreases along a period from left to right due to the different states of orbitals, volume effects and electronegativity of the atoms. The interaction energy between V_{ZZ} and the nuclear electric quadrupole moment eQ at the sites of the quadrupole nuclei is measured by C_Q, while the asymmetry parameter η measures the deviation from the cylindrical symmetry at the sites of the quadrupole nuclei. The value of η varies for different compounds and elements. The EFG and the

Table V. The calculated valence H_{hf}^{val}, core H_{hf}^{cor} and H_{hf}^{dip} contributions of the UX_3 and the total $|H_{hf}^{tot}|$ at U, In, Tl and Pb atoms in (kGauss), and EFG within exchange–correlation functional GGA + U, before and after applying the SOC coupling with asymmetry parameters with Q (barns)

Potential	Site	$\lvert H_{hf}^{tot}\rvert$	H_{hf}^{val}	H_{hf}^{cor}	H_{hf}^{dip}	H_{hf}^{orb}	EFG	ASYM	Q (barn)	
UIn_3	U	4722.75	666.424	− 1014.666	− 271.250	− 4103.26	− 2.63700	0.00000		
	In	− 136.924	− 142.815	− 0.37600	6.96250	− 0.69580	12.0732	0.02399		
UTl_3	U	− 5034.73	709.901	− 1081.90	− 266.230	− 4396.50	− 2.53300	0.00000		
	Tl	− 251.024	− 291.672	− 1.12700	19.4346	22.3400	35.8940	0.00370		
UPb_3	U	− 4401.07	605.337	− 913.914	− 201.320	− 4290.50	− 1.74970	0.00000		
	Pb	− 230.424	− 221.760	− 1.24300	− 7.61850	0.19700	33.3543	0.00909		
UIn_3	U	− 4800.39	669.437	− 1022.86	− 268.800	− 4114.00	− 2.54800	0.00000		
	In	− 136.188	− 144.460	− 0.37200	7.70000	0.95000	15.5500	0.18600	0.77[a]	
UTl_3	U	− 5035.06	709.902	− 1081.92	− 266.240	− 4396.80	1.95000	0.00000		
	Tl	− 247.461	− 291.660	− 1.128 00	19.4300	25.8970	36.5260	0.18890	0.74[a]	
UPb_3	U	− 4998.77	607.231	− 916.304	− 203.200	− 4486.50	0.69200	0.00000		
	Pb	− 227.555	− 221.830	− 1.32800	− 7.57800	3.18300	34.9400	0.44000	− 0.34[a]	52%

[a]Reference 42.

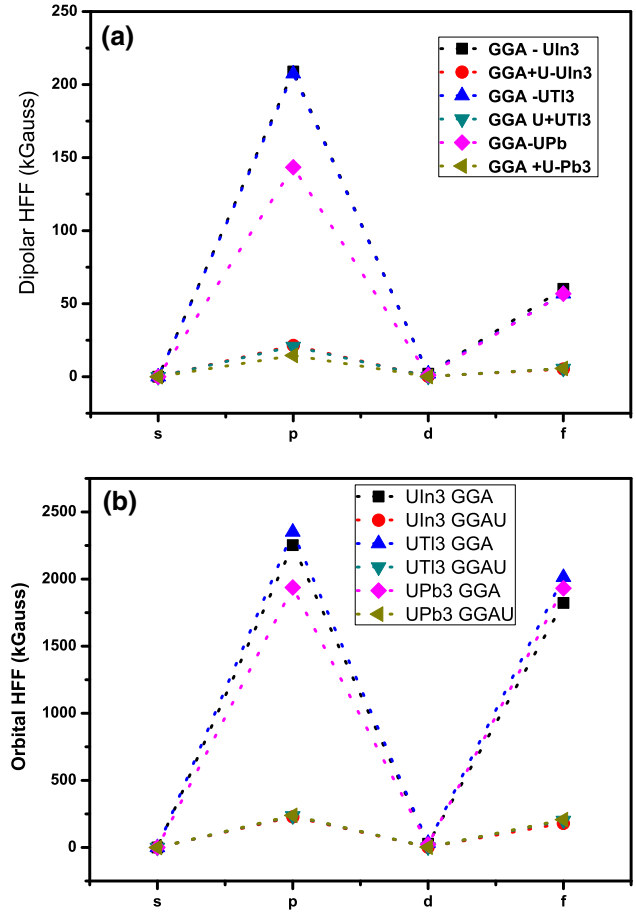

Fig. 6. (a) Contribution of dipolar HFF of individual orbital. (b) Contribution of each sub-shell in orbital hyperfine field.

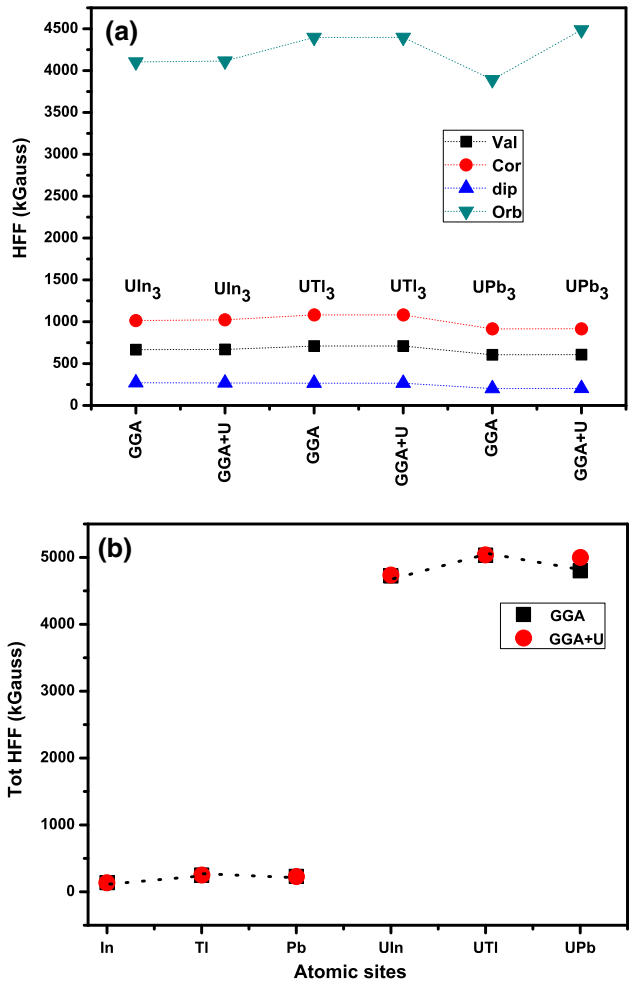

Fig. 7. (a) Valence, core, dipolar and orbital hyperfine fields of UX_3 (In, Tl, Pb) by GGA and GGA + U + SOC. (b) Total hyperfine fields at uranium and indium, thallium and lead in kGauss.

asymmetry term of the post-transition metals are large, and they deviated from the cylindrical symmetry to a greater extent. The asymmetry parameter calculated by GGA + U is directly related to the lattice constant, which is in accord with separate studies.[17–52] The calculated values of EFG at the uranium sites enable measurement of the electric quadrupole moment of the uranium atom, which is a nuclear parameter that is important in nuclear physics. Using the magnetic hyperfine interaction energy derived from NMR or NQR in conjunction with the relationship $E_{HFF} = \mu HFF$, one can easily calculate the nuclear magnetic moment. Similarly, by using the electric quadrupole interaction energy, $h\upsilon_Q = e^2qQ$ one can calculate the electric quadrupole moment of the quadrupole nuclei. Hence, HFF and EFG should be considered when measuring the nuclear magnetic moment of uranium, indium, thallium and lead nuclei as well as the nuclear electric quadrupole moment of the nucleus.

CONCLUSIONS

We have used density functional theory to calculate the structural, electronic, magnetic and hyperfine fields and the electric field gradient of bulk cubic UX_3 [X = In, Tl, Pb]. For the bulk calculations, we have used LDA and PBE-GGA with an additional Hubbard-*U* term, GGA + U, for the treatment of heavy fermions along with the HF-PBEsol hybrid functional. The lattice parameters calculated by LDA and PBE-GGA were found to be in agreement with the available experimental data, while the magnetic moments were more accurately predicted by GGA + U+SOC. The electronic specific heat for UTl_3 was calculated using a different functional. The Hill limit and magnetic moment at the uranium site in UIn_3, UTl_3, and UPb_3 calculated using GGA + U and HF-PBEsol with SOC suggest that the 5f electrons are delocalized at the uranium atomic sites. The hyperfine field, electric field gradient and nuclear quadrupole coupling constant have been investigated for these compounds. It was found that the hyperfine field increased from top to bottom for the UX_3 family. The major contribution arises from the orbital hyperfine field. The computed C_Q increased from top to bottom and decreased along the period from left to right due to the different orbitals. The HFF, EFGs, and C_Q at the U site originate primarily from f and p states, while the p state is predominant at post-transition atomic sites.

REFERENCES

1. V. Sechovsky and L. Havela, *Ferromagnetic Materials*, 4th ed. (Amsterdam: North-Holland, 1988).
2. D.D. Koelling, B.D. Dunlap, and G.W. Crabtree, *Phys. Rev. B* 31, 4966 (1985).
3. A.E. Dwight, *Developments in the Structural Chemistry of Alloy Phases*, ed. B.C. Giessen (New York: Plenum, 1969), pp. 181–226.
4. E.A. Kmetko and H.H. Hill, *Plutonium 70*, ed. W.N. Miner (New York: AIME, 1970), p. 233.
5. B. Johansson, *Phys. Rev. B* 8, 2740 (1975).
6. Y. Gao, B. Wang, Y. Lei, B. Teo, and Z. Wang, *Nano Res.* 9, 622 (2016).
7. Y. Gao and Z. Wang, *Chin. Phys. B* 25, 083102 (2016).
8. E. Ghasemikhah, S. Jalali Asadabadi, I. Ahmad, and M. Yazdani-Kacoei, *RSC Adv.* 5, 7592 (2015).
9. D. Aoki, N. Suzuki, K. Miyake, Y. Inada, R. Settai, K. Sugiyama, and E. Yamamoto, *J. Phys. Soc. Jpn.* 70, 538 (2001).
10. M. Loewenhaupt and C.K. Loong, *Phys. Rev. B* 41, 9294 (1990).
11. Y. Tokiw, A.D. Aoki, Y. Haga, E. Yamamoto, S. Ikeda, R. Settai, A. Nakamura, and Y.O. Nuki, *J. Phys. Soc. Jpn.* 70, 3326 (2001).
12. M.H. Maaren, H.J. Daal, K.H.J. Buschow, and C.J. Schinkel, *Solid State Commun.* 14, 145 (1974).
13. A. Murasik, J. Leciejewicz, S. Ligenza, and A. Misiuk, *Phys. Status Solidi A* 20, 395 (1973).
14. A. Murasik, P. Fisher, and Z. Zolnierek, *Physica B + C* 102, 188 (1980).
15. S. Jalali-Asadabadi, S. Cottenier, H. Akbarzadeh, R. Saki, and M. Rots, *Phys. Rev. B* 66, 195103 (2002).
16. S. Jalali-Asadabadi and H. Akbarzadeh, *Physica B* 349, 76 (2004).
17. S. Jalali-Asadabadi, *Phys. Rev. B* 75, 205130 (2007).
18. M. Yazdani-Kachoei, S. Jalali-Asadabadi, A. Iftikhar, and Z. Kourosh, *Sci. Rep.* 6, 31734 (2016).
19. K. Schwarz, P. Blaha, and G. Madsen, *Comput. Phys. Commun.* 147, 71 (2002).
20. A. Andreev, V.K. Belov, A. Deriagin, V.Z.A. Kazeĭ, R.Z. Levitin, A. Meňovský, Y. Popov, and V.I. Silant'ev, *JETP* 48, 1187 (1978).
21. P. Blaha, K. Schwarz, G.K.H. Madsen, D. Kvasnicka, and J. Luitz, *WIEN2K: An Augmented Plane Wave plus Local Orbitals Program for Calculating Crystal Properties* (Vienna: Vienna University of Technology, 2001).
22. J.P. Perdew and A. Zuanger, *Phys. Rev. B* 23, 5048 (1981).
23. J.P. Perdew, K. Burke, and M. Ernzerhop, *Phys. Rev. Lett.* 77, 3865 (1996).
24. V.I. Anisimov, I.V. Solovyev, M.A. Korotin, M.T. Czyzyk, and G.A. Sawatzky, *Phys. Rev. B* 48, 16929 (1993).
25. S.L. Dudarev, G.A. Botton, S.Y. Savrasov, C.J. Humphreys, and A.P. Sutton, *Phys. Rev. B* 57, 1505 (1998).
26. V.I. Anisimov and O. Gunnarsson, *Phys. Rev. B* 43, 7570 (1991).
27. M.P. Johansson, D. Sundholm, G. Gerfen, and M. Wikström, *J. Am. Chem. Soc.* 39, 11771 (2002).
28. A.D. Becke, *J. Chem. Phys.* 98, 5648 (1993).
29. A.D. Becke, *Phys. Rev. A* 38, 3098 (1988).
30. C. Lee, W. Yang, and R.G. Parr, *Phys. Rev. B* 37, 785 (1988).
31. F. Birch, *Phys. Rev. B* 71, 809 (1947).
32. K. Schwarz and P. Blaha, *Comput. Mater. Sci.* 28, 259 (2003).
33. J. Kollar, L. Vitos, and H.L. Skriver, *Phys. Rev. B* 55, 15353 (1997).
34. S. Raju, E. Mohandas, and V.S. Raghunathan, *J. Phys. Chem. Solids* 58, 1367 (1997).
35. H.H. Hill, *Plutonium 1970 and Other Actinides, Part I, Nuclear Metallurgy*, vol. 17, ed. W.N. Miner (New York: The Metallurgical Society, 1970), p. 2.
36. C. Kittle, *Introduction to Solid State Physics* (New York: John Wiley, 1983).
37. Y. Tokiwa, D. Aoki, Y. Haga, E. Yamamoto, S. Ikeda, R. Settai, A. Nakamura, and Y. Onuki, *J. Phys. Condens. Matter* 26, 036001 (2013).
38. M.S.S. Brooks and P.J. Kelly, *Phys. Rev. Lett.* 51, 1708 (1983).
39. M.S.S. Brooks, *Physica B* 190, 55 (1993).
40. G. Kalvius, J. Gal, F. Litterst, W. Potzel, J. Moser, U. Potzel, W. Schiessl, S. Zwirner, S. Fredo, and S. Tapuchi, *J. Phys. Colloq.* 49, 477 (1988).
41. M.B. Brodsky, *Prog. Phys.* 41, 1457 (1978).
42. N.J. Stone, *Atom. Data Nucl. Data Tables* 111–112, 1 (2016).
43. P. Novak, *Calculation of Hyperfine Field in WIEN2k* (Prague 6, Czech Republic: Institute of Physics of ASCR, 2006).

44. D. Torumba, P. Novák, and S. Cottenier, *Phys. Rev. B* 77, 155101 (2008).
45. S. Zhu, X. Li, Z. Lu , G. Wang, and W. Shu, *Application of Nuclear Quadrupole Resonance to Detection of Explosives and Research Activities at CIAE* (Beijing: China Institute of Atomic Energy, 2008).
46. S.K. Mohanta, S.N. Mishra, S.K. Srivastava, and M. Rots, *Solid State Commun.* 150, 1789 (2010).
47. P. Ravindran, A. Delin, P. James, B. Johansson, J.M. Wills, R. Ahuja, and O. Eriksson, Magnetic. *Phys. Rev. B* 59, 15680 (1999).
48. M. Jamal, S.J. Hashemifar, and H. Akbarzadeh, *J. Magn. Magn. Mater.* 322, 3841 (2010).
49. M. Divis, K. Schwarz, P. Blaha, G. Hilscher, H. Michor, and S. Khmelevskyi, *Phys. Rev. B* 62, 67 (2000).
50. Z. Nourbakhsh, H. Akbarzadeh, and A. Pourghazi, *J. Phys. Condens. Matter* 17, 2407 (2005).
51. M. Rafiee and S. Jalali-Asadabadi, *Comput. Mater. Sci.* 47, 584 (2009).
52. R. Jonathan, C. Yates, J. Pickard, and C.M. Payne, *J. Phys. Chem. A* 108, 6032 (2004).